Journal of Hazardous Materials 321 (2017) 745–752

Contents lists available at ScienceDirect

Journal of Hazardous Materials

journal homepage: www.elsevier.com/locate/jhazmat

Stabilization of mercury over Mn-based oxides: Speciation and reactivity by temperature programmed desorption analysis

Haomiao Xu[a], Yongpeng Ma[b], Wenjun Huang[a], Jian Mei[a], Songjian Zhao[a], Zan Qu[a], Naiqiang Yan[a,*]

[a] School of Environmental Science and Engineering, Shanghai Jiao Tong University, Shanghai 200240, China
[b] Henan Collaborative Innovation Center of Environmental Pollution Control and Ecological Restoration, Zhengzhou University of Light Industry, No. 136, Science Avenue, Zhengzhou 450001, China

HIGHLIGHTS

- Hg-TPD method was used for speciation of mercury species.
- Different elements modified MnOx have different mercury binding state.
- Understanding mercury existed state was beneficial for designing novel materials.

GRAPHICAL ABSTRACT

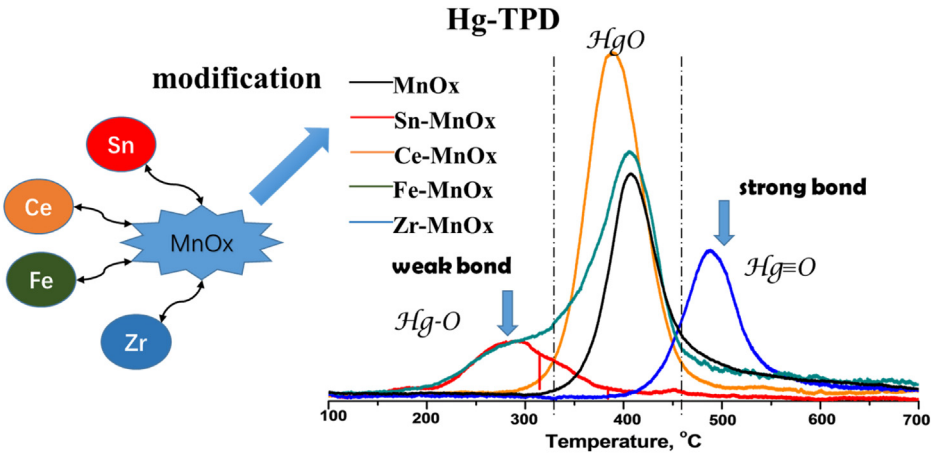

ARTICLE INFO

Article history:
Received 12 July 2016
Received in revised form
12 September 2016
Accepted 13 September 2016
Available online 14 September 2016

Keywords:
Elemental mercury
Manganese oxides
Adsorption
Mercury species

ABSTRACT

Mercury temperature-programmed desorption (Hg-TPD) method was employed to clarify mercury species over Mn-based oxides. The elemental mercury (Hg^0) removal mechanism over MnO_x was ascribed to chemical-adsorption. HgO was the primary mercury chemical compound adsorbed on the surface of MnO_x. Rare earth element (Ce), main group element (Sn) and transition metal elements (Zr and Fe) were chosen for the modification of MnO_x. Hg-TPD results indicated that the binding strength of mercury on these binary oxides followed the order of Sn-MnO_x < Ce-MnO_x ~ MnO_x < Fe-MnO_x < Zr-MnO_x. The activation energies for desorption were calculated and they were 64.34, 101.85, 46.32, 117.14, and 106.92 eV corresponding to MnO_x, Ce-MnO_x, Sn-MnO_x, Zr-MnO_x and Fe-MnO_x, respectively. Sn-MnO_x had a weak bond of mercury (Hg-O), while Zr-MnO_x had a strong bond (Hg≡O). Ce-MnO_x and Fe-MnO_x had similar bonds compared with pure MnO_x. Moreover, the effects of SO_2 and NO were investigated based on Hg-TPD analysis. SO_2 had a poison effect on Hg^0 removal, and the weak bond of mercury can be easily destroyed by SO_2. NO was favorable for Hg^0 removal, and the bond strength of mercury was enhanced.

* Corresponding author.
E-mail address: nqyan@sjtu.edu.cn (N. Yan).

http://dx.doi.org/10.1016/j.jhazmat.2016.09.030
0304-3894/

1. Introduction

Mercury (Hg) is a hazardous element in the environment [1,2]. Among various anthropogenic mercury emission sources, coal-fired power plant was regarded as the largest one [3,4]. In the coal-fired flue gas, mercury existed as elemental mercury (Hg^0), oxidized mercury (Hg^{2+}) and particle-bond mercury (Hg^p). Hg^0 was hard to be removed due to its insolubility and high volatility [5]. Currently, two available methods were developed for Hg^0 removal, they are catalytic oxidation (Hg^0 to Hg^{2+}) and adsorption (Hg^0 to Hg^p) methods [6–8]. Hg^{2+} can be captured in the wet flue gas desulfurization system. However, mercury enriched in the slurry could cause secondary contamination. Therefore, adsorption technology seemed as a potential method for Hg^0 removal.

Active carbon (AC) was an efficient material for gaseous pollutants elimination, and it was used as a sorbent for Hg^0 removal [5,9]. However, AC was limited for a wide usage in the coal-fired power plants due to its high cost. In addition, AC does not have high Hg^0 capture capacity and it highly depends on halogen species in the flue gas [10,11]. The chemical-adsorbed Hg-Cl or Hg-Br could increase the Hg^0 capacities. Some studies used Cl^- or Br^- modified AC to enhance the Hg^0 removal efficiency [12–14]. However, the cost was also increased. Recently, transition metal oxides (such as FeO_x, CuO_x, MnO_x and CoO_x) were selected for Hg^0 removal [15]. The primary Hg^0 removal mechanism over these metal oxides was ascribed to chemical adsorption [15,16]. Hg^0 was firstly oxidized to Hg^{2+}, followed by the adsorption of Hg^{2+} with the surface oxygen.

Among efficient mercury adsorbents, MnO_x was the most promising one due to its high redox potential, environmental friendliness and low cost [16–18]. To enhance Hg^0 removal performance, modified MnO_x were developed. Ce-MnO_x enhanced surface oxygen storage capacity and enlarged Hg^0 capacity [19]. Sn-MnO_x enlarged the reaction temperature window [20]. Fe-MnO_x protected Mn active sites from the poison of SO_2 [21]. Zr-MnO_x also enhanced the Hg^0 capture capacities [22]. These Mn-based oxides vary from the performances, but Hg^0 removal mechanism can be described as follows: 1) gaseous Hg^0 was firstly adsorbed on the surface of Mn-based oxide; 2) then adsorbed Hg^0 was oxidized to Hg^{2+} due to high valance of Mn (Mn^{4+} or Mn^{3+}); and 3) the Hg^{2+} combined with surface oxygen of Mn-based oxide. During this chemical-adsorption process, mercury changed to oxidized state and combined with surface oxygen. However, to our knowledge, few researches focus on the binding state of mercury on the surface of MnO_x. Insight into the speciation and reactivity of mercury were beneficial for better understanding the Hg^0 removal mechanism and further modification of MnO_x.

Mercury temperature-programmed desorption (Hg-TPD) method was employed for thermal decomposition of mercury in our previous studies. In addition, it is a method for the speciation of mercury. Wu et al. observed the reactivity of HgO over activated carbon by Hg-TPD analysis [23]. Different mercury species formed in the presence of HCl and SO_2. The speciation of mercury in fly ashes were studied by Lopez-Anton et al. using Hg-TPD analysis [24]. The results provide valuable information for understanding mercury retention mechanism. Hg-TPD is a meaningful method to identify mercury species, to investigate the Hg^0 removal mechanism and to further design effective adsorbent for mercury [23,25].

Here, in this study, Hg-TPD method was employed to explore the mercury removal mechanism over Mn-based metal oxides. The Hg^0 removal performances of AC and various modified MnO_x were evaluated using a fix-bed adsorption system. The effects of SO_2 and NO on mercury species were also investigated. Furthermore, activation energies for desorption were calculated based on thermodynamic calculation.

2. Experimental methods

2.1. Sorbent preparation

Mn-based metal oxides were prepared using co-precipitation method. Suitable amounts of $Ce(NO_3)_4$, $SnCl_4$, $Zr(NO_3)_4$, $Fe(NO_3)_3$ and $Mn(NO_3)_2$ were dissolved in distilled water. The molar ratios of Ce: Mn, Sn: Mn, Zr: Mn and Fe: Mn were 1:1. After stirring for 30 min, a stoichiometric amount of ammonia was added to the mixture as the precipitation agent under strong stirring for 1 h. Then the precipitate was filtered and washed with deionized water three times to remove Cl^- from the precipitate. Lastly, the precipitate was transferred to a muffle furnace and calcined at 500 °C for 5 h. All of the samples were ground to a 40–60 mesh size. For comparison, granular active carbon was used in this study.

2.2. Material characterizations

The Brunauer–Emmett–Teller (BET) surface area was calculated based on a multipoint adsorption-desorption method, which was analyzed using a N_2 sorption measurement (Nova-2200 e) at 77 K. The pore diameter and pore volume were calculated based on the Barrett–Joyner–Halenda (BJH) method. X-ray photoelectron spectroscopy (XPS, Shimadzu–Kratos) was used to examine the valance states of the elements on the surface of the materials. This instrument coupled with an ultra DLD spectrometer with an Al Kα excitation source. The C 1 s line at 284.6 eV was employed as a reference for the binding energy calibration.

2.3. Hg^0 adsorption performance

The Hg^0 removal performances were evaluated using a fixed-bed reactor, and a schematic representation of the Hg^0 adsorption system is shown in Fig. S1. Hg^0 vapor was generated by a Hg^0 permeation tube and carried by pure N_2. Various gases including N_2, O_2, SO_2, and NO were introduced to the inlet of the gas mixer. The flow rate of each gas was controlled by mass flow controllers (MFC) and the total flow rate was 500 ml/min. The as-prepared Mn-based oxides were set in a fixed-bed reactor system. The reaction temperature was controlled from 50 to 350 °C by a temperature controller tubular furnace. A cold vapor atomic absorption spectroscopy (CVAAS) analyzer was employed as an online continuous detector that could only detect Hg^0. The concentration of Hg^0 was measured using Lumex RA 915+. During each adsorption test, the mass of the sorbent was 20 mg. The inlet concentration of Hg^0 was 500 μg/m^3. At the beginning of each test, the simulated gas bypassed the reactor and the inlet gas was detected to ensure a stable Hg^0 concentration. Then the simulated gas passed the samples and the Hg^0 concentration was detected by CVAAS online system. After adsorption a period of time, the Hg^0 adsorption capacities were calculated according to Eq. (1):

$$Q = \frac{1}{m}\int_{t2}^{t1}\left(\frac{Hg^o_{in} - Hg^o_{out}}{Hg^o_{in}}\right) * f * \mathrm{d}t \quad (1)$$

where Q is the Hg^0 adsorption capacity, m is the mass of the sorbent in the fixed-bed, f is the flow rate of the influent, and t_1 and t_2 are the initial and final test times, respectively, of the breakthrough curves.

2.4. Mercury temperature programed desorption experiment

Mercury temperature programmed desorption (Hg-TPD) method was developed to evaluate the desorption performance of as-prepared Mn-based metal oxides. Prior to each test, the

sorbents were adsorbed for 30 min at 150 °C with N_2 + 4% O_2. After that, the sorbent was bypassed pure N_2 until the Hg^0 base line was stable. After the furnace cooled to 100 °C, the temperature increased from 100 to 700 °C in a pure N_2 carrier gas. The heating rates were set to 2, 5 and 10 °C/min. The mercury signal was recorded by a CVAAS online system. To investigate the effects of SO_2 and NO, the $SO_2 + O_2$ + Hg-TPD and NO + O_2 + Hg-TPD were detected. During the adsorption test, the concentration of O_2, SO_2 and NO were 4%, 500 ppm and 500 ppm, respectively. The flow rate was kept 500 ml/min.

3. Results and discussion

3.1. Hg^0 removal performance over AC and MnO_x

As shown in Fig. 1, the Hg^0 removal performances of traditional active carbon (AC) and MnO_x were tested. AC had only approximately 50% Hg^0 removal efficiency in the initial several minutes, and it gradually lost its Hg^0 removal performance. After 600 min reaction, AC completely lost the Hg^0 removal performance. However, MnO_x had a higher Hg^0 removal performance compared to that of AC. The Hg^0 removal efficiency was increased by about 30%. After 600 min reaction, MnOx still had higher than 30% Hg^0 removal efficiency. Obviously, MnO_x had a better Hg^0 removal performance than AC.

As shown in Fig. 2, the XPS spectra of spent AC and MnO_x were illustrated. (The spent AC or MnOx refers to the materials are used after the adsorption reaction) Fig. 2(a) shows the C 1s of spent AC, the peaks at 288.6, 285.8 and 284.7 eV were ascribed to O—C=O groups, C—O groups (epoxy and alkoxy) and C—C/C=C groups in aromatic rings, respectively [17,26]. For O 1s of AC (Fig. 2(b)), a wide peak centered at 533.6 eV was ascribed to the surface oxygen of AC [17]. For Hg 4f of AC (Fig. 2(c)), it existed a peak at 105.5 eV, which corresponds to the adsorbed mercury on the surface of AC. For Mn 2p of MnO_x, as shown in Fig. 2(d), the peaks at 643.6 and 641.8 eV were ascribed to Mn^{4+} and Mn^{3+}, respectively [18]. Based on our previous studies, in the Hg^0 removal process, Mn was the primary active site for Hg^0 oxidation [17,18]. After Hg^0 was oxidized to Hg^{2+}, Hg^{2+} combined with the surface oxygen on its surface. As shown in Fig. 2(e), the O 1 s spectra of MnO_x was illustrated, the peaks at 532.8 and 530.1 eV were ascribed to surface oxygen (O_{sur}) and lattice oxygen (O_{latt}), respectively [18,19]. The O_{latt} plays an important role for the structure of manganese oxide. While the O_{sur} was the binding site for the oxidized mercury. As shown in Fig. 2(f), the peaks at 105.4 and 101.3 eV were assigned to the oxidized mercury [17,21]. The results indicated that the mechanism for Hg^0 removal over MnO_x was chemical-adsorption, in which the Hg^0 was firstly oxidized to Hg^{2+}.

3.2. Comparison of Hg-TPD spectra of AC and MnO_x

As illustrated in Fig. 3, the Hg-TPD curves of AC and MnO_x were collected under different heating rates. Obviously, mercury could release from the surface of AC at low temperature compared to that of MnO_x. As shown in Fig. 3(a), under a heating rate of 2 °C/min, mercury released from the surface of AC at 150 °C, an obvious peak centered at 201.2 °C. When the temperature was higher than ~300 °C, mercury curve become flat, indicated that mercury absolutely desorbed from the surface of AC. However, for MnO_x, it exhibited quite a different desorption performance, mercury began release from the surface of MnO_x at approximately 300 °C, and it had a strong peak at 347.6 °C. When the temperature was higher than 500 °C, almost all mercury released from the surface of MnO_x. Obviously, it exhibited different desorption performance between AC and MnO_x.

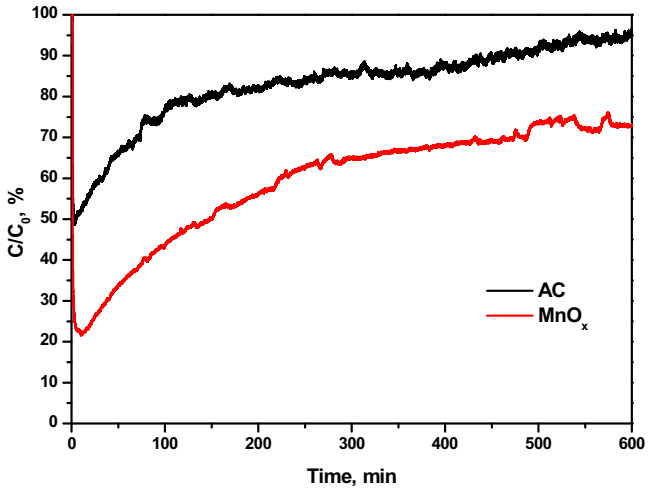

Fig. 1. Hg^0 adsorption performance of AC and MnO_x. Mass of sorbents: 20 mg; adsorption temperature:150 °C; total flow rate: 500 ml/min and gas components: 4% O_2.

As shown in Table 1, the BET surface areas of AC and MnO_x were 312.6 and 5.4 m^2/g, respectively. The larger surface area of AC didn't result in higher Hg^0 adsorption capacity. Based on the above results, the mechanism for Hg^0 removal over AC can be ascribed to a physical-adsorption process. Firstly, gaseous mercury adsorbed on the surface of AC due to its high surface area. Then mercury combined with AC with a weak physical bond, the equation can be described as follows:

$$Hg(g) \rightarrow Hg(ads) \quad (2)$$

$$Hg(ads) \rightarrow Hg\text{--}AC(ads) \quad (3)$$

where "–" represents the physical-adsorption bond between Hg and AC.

However, the Hg^0 removal mechanism for MnO_x was ascribed to chemical-adsorption. As discussed in various previous studies, the mechanism was ascribed to a Mars-Maessen mechanism. The oxidized mercury combined with adsorbed oxygen of MnO_x, and that the oxygen can be supplied by O_2 from the flue gas. The mechanism can be described as follows: [15,16]

$$Hg(ads) + MnO_x \rightarrow HgO(ads) + MnO_{x-1} \quad (4)$$

$$MnO_{x-1} + 1/2O_2 \rightarrow MnO_x \quad (5)$$

$$HgO(ads) + MnO_x \rightarrow HgMnO_{x+1} \quad (6)$$

3.3. Mercury desorption activation energy calculation

The chemical-adsorption could enhance the Hg^0 adsorption capacities of MnO_x. The biding strength can be described by the mercury desorption activation energy. As shown in Fig. 2(b) and (c), the Hg-TPD curves were collected under heating rates of 5 and 10 °C/min, respectively. When the heating rate was 5 °C/min, it existed a delayed effect for mercury releasing from the surface. The desorption temperatures were 229.7 and 406.7 °C for AC and MnO_x, respectively. Similarly, when the heating rate was 10 °C/min, the desorption peak further delayed. The desorption temperatures were 274.7 and 403.9 °C for AC and MnO_x, respectively. Based on Hg-TPD data, mercury desorption activation energy can be calculated.

After adsorption, mercury enriched in the spent sorbent could cause mercury secondary contamination. Mercury can release from the surface of the spent sorbents. After thermal-desorption, the released mercury can be collected along with gas temperature

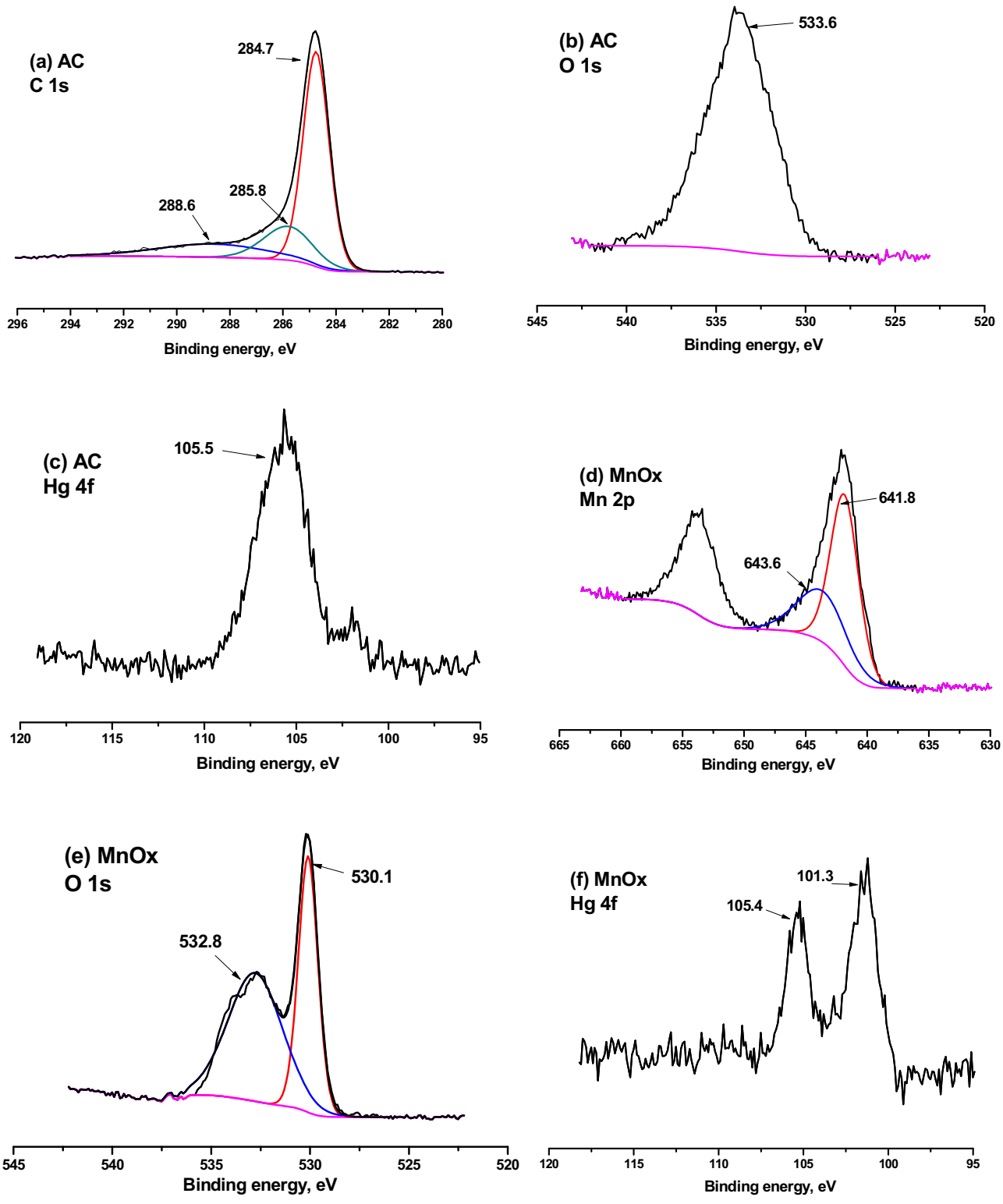

Fig. 2. XPS analysis of spent AC and MnO_x.

decreased. The mercury desorption activation energy (E_d) was calculated which was based on intrinsic kinetic model. The model assumed that the desorption process follows first-order kinetics:

$$\frac{r_d}{N_s} = -\frac{d\theta}{dt} = k_d\theta \quad (7)$$

where r_d is desorption rate of mercury from sorbent (mol/min), Ns denotes the maximum mercury concentration on unit surface of sorbent (mol/cm^2), θ denotes the transient coverage of mercury and t is the time (min), k_d is the desorption rate coefficient and defined as follows:

$$k_d = A\exp\left(-\frac{E_d}{RT}\right) \quad (8)$$

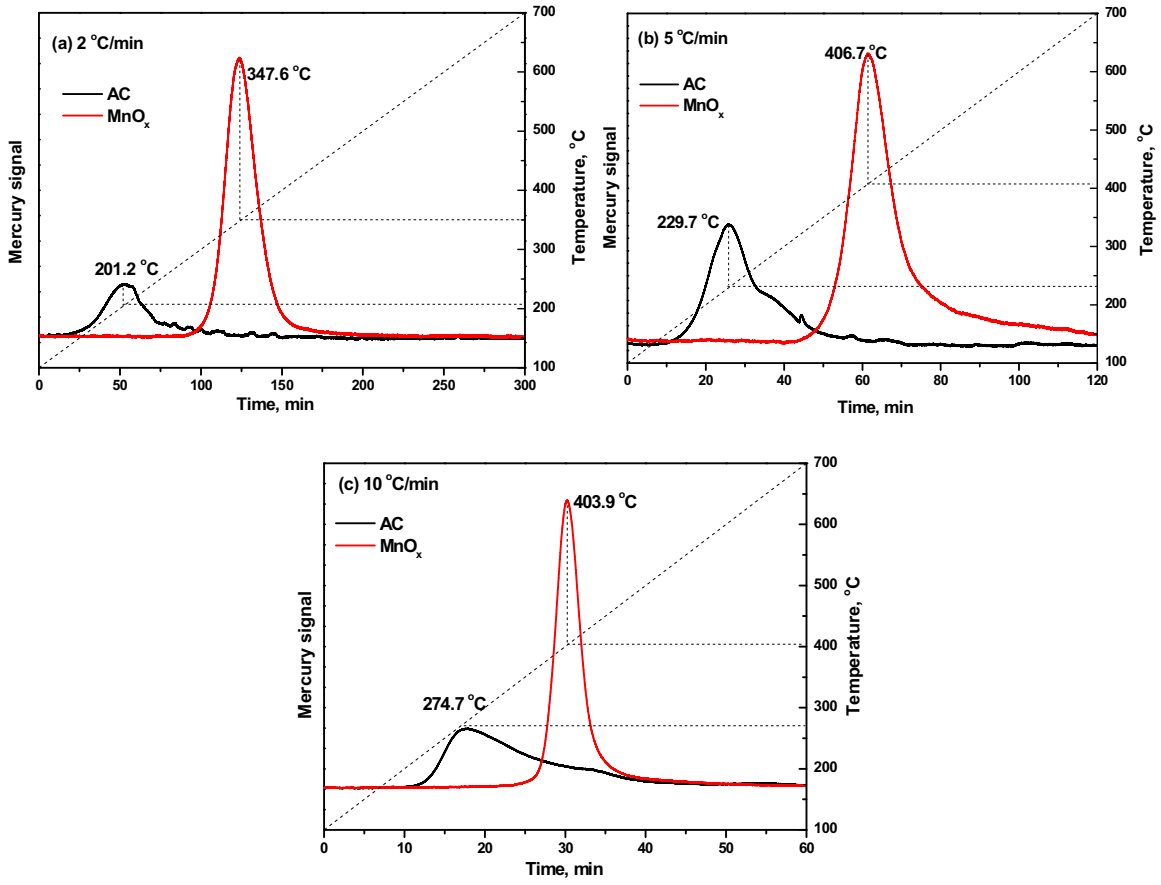

Fig. 3. Hg-TPD curves over AC and MnO_x under the different heating rates: (a) 2 °C/min, (b) 5 °C/min and (c) 10 °C/min.

Table 1
Calculation of mercury desorption activation energy from Mn-based oxides surface.

Materials	BET surfaces areas (m^2/g)	600 min adsorption capacity (mg/g)	The peak temperatures(T_p, °C) for different heating rates, β (°C/min)			Activation energy for desorption (KJ/mol)
			2 °C/min	5 °C/min	10 °C/min	
AC	312.6	1.3	201.2	229.7	274.7	38.12
MnO_x	5.4	2.1	347.6	406.7	403.9	64.34
Ce-MnO_x	112.3	6.0	357.6	388.4	408.2	101.85
Sn-MnO_x	53.9	3.5	286.5	294.8	355.1	46.32
Zr-MnO_x	148.9	5.0	428.4	465.0	481.2	117.14
Fe-MnO_x	21.9	3.3	392.4	406.6	442.5	106.92

where E_d is the desorption activation energy (kJ/mol), R is gas constant, T is temperature, A is pre-exponential factor. Combining Eqs. (7) and (8), Eq. (9) could be obtained.

$$\frac{r_d}{N_s} = -\frac{d\theta}{dt} = A\theta\exp\left(-\frac{E_d}{RT}\right) \quad (9)$$

Assumed that the initial temperature of TPD experiment was T_0 (K), and the heating rate was β (K/min), so reaction temperature varied with time following Eq. (10):

$$T = T_0 + \beta t \quad (10)$$

With the elevation of temperature, mercury on sorbent surface desorbs gradually. Assumed that the desorption rate reaches the maximum value at a certain temperature T_p (K), then $\frac{dr_d}{dt} = 0$, and time derivative of equation (9) can be expressed by Eq. (11):

$$\frac{1}{N_s}\frac{dr_d}{dt} = A\frac{d\theta}{dt}\exp-\frac{E_d}{RT_p} + A\theta\frac{E_d}{R}\frac{1}{T_p^2}\exp\left(-\frac{E_d}{RT_p}\right)\frac{dT}{dt} = 0 \quad (11)$$

Combining with Eq. (10), Eq. (11) could be written as Eq. (12):

$$\ln\frac{\beta}{RT_p^2} = -\frac{E_d}{RT_p} - \ln\frac{E_d}{A} \quad (12)$$

Eq. 12 can be further revised as Eq. (13):

$$2\ln T_p - \ln\beta = \frac{E_d}{RT_p} + \ln\frac{E_d}{AR} \quad (13)$$

Based on Hg-TPD curves under different heating rates, making plot of $(2\ln T_p - \beta)$ against $\frac{1}{T_p}$, a linear relation can be generated. According to slope and intercept, E_d and A could be calculated and the result was listed in Table 1. The activation energy of desorption for AC and MnO_x were 38.12 and 64.34 KJ/mol, respectively. The higher activation energy indicated the strong bond between mercury and the adsorbent.

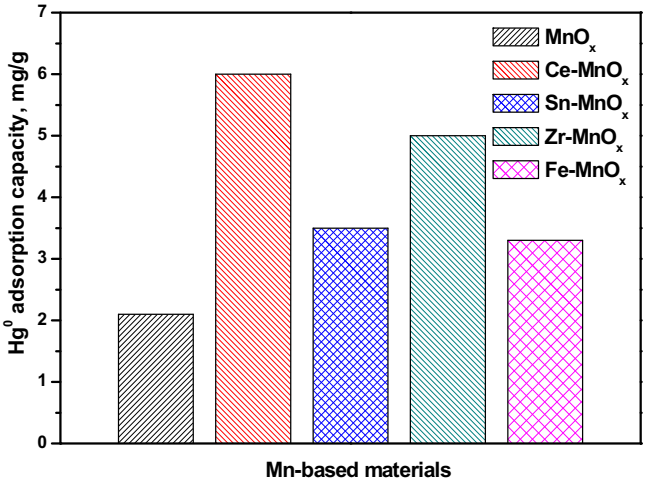

Fig. 4. The Hg^0 removal capacities of various Mn-based sorbents. Mass of sorbents: 20 mg; adsorption temperature: 150 °C; total flow rate: 500 ml/min and gas components: 4% O_2.

3.4. Various Mn-based metal oxides for Hg^0 adsorption and Hg-TPD spectra

Various elements were selected for modification of MnO_x to enhance Hg^0 removal performance. Ce, Sn, Zr and Fe were often selected based on literatures reports. The Hg^0 removal performances of these modified materials were tested and their 600 min Hg^0 adsorption capacities were presented in Fig. 4. Pure MnO_x had only 2.1 mg/g capacity. Ce is rare earth element and CeO_2 has excellent oxygen storage capacity. The abundant surface oxygen was beneficial for Hg^0 capture. The surface area of Ce-MnO_x was 112.3 m^2/g which was much larger than that of pure MnO_x. Ce-MnO_x had the largest Hg^0 capacity and it was ~6 mg/g Hg^0 adsorption capacity. Sn was the main group element and SnO_2 was often used as semi-conductor. SnO_2 had super electrons transfer performance. The Hg^0 adsorption capacity of Sn-MnO_x was 3.5 mg/g. Zr was the transition metal element and ZrO_2 was often used as catalyst support. ZrO_2 benefits for the dispersion of MnO_x particles. It had the largest surface area of 148.9 m^2/g among the as-prepared Mn-based oxides. The Hg^0 adsorption capacity of Zr-MnO_x was 5.0 mg/g. Fe was active transition metal and FeO_x had catalytic oxidation performance for Hg^0. The composite of Fe-MnO_x further increased the Hg^0 adsorption capacity, it was approximately 3.3 mg/g after 600 min reaction.

The Hg-TPD spectra of these Mn-based binary oxides were presented in Fig. 5, and it showed the curves under the heating rate of 5 °C/min. For Ce-MnO_x, mercury began released from the surface of Ce-MnO_x at ~200 °C and a peak centered at approximately 388.4 °C. When the temperature was higher than 500 °C, all the surface mercury released from Ce-MnO_x surface. The peak position was close to that of pure MnO_x. It indicated that the mercury species was the same to the pure MnO_x. However, for Sn-MnO_x, mercury began release at 200 °C and the desorption peak centered at 286.5 °C which was lower than that of pure MnO_x. But the temperature was higher than that of AC. It was speculated that mercury on the surface of Sn-MnO_x existed as a form of weak-binding state. For Zr-MnO_x, the desorption peak centered at 485.0 °C, which was a much higher than that of pure MnO_x. The results reflected that the strong-binding state of mercury on the surface of Zr-MnO_x. For Fe-MnO_x, the desorption peak centered at 406.6 °C which was a little higher than that of pure MnO_x. In addition, there existed a weak peak on the Hg-TPD curve of Fe-MnO_x, indicating that the weak-binding and strong binding state of mercury co-existed on the surface of Fe-MnO_x after adsorption.

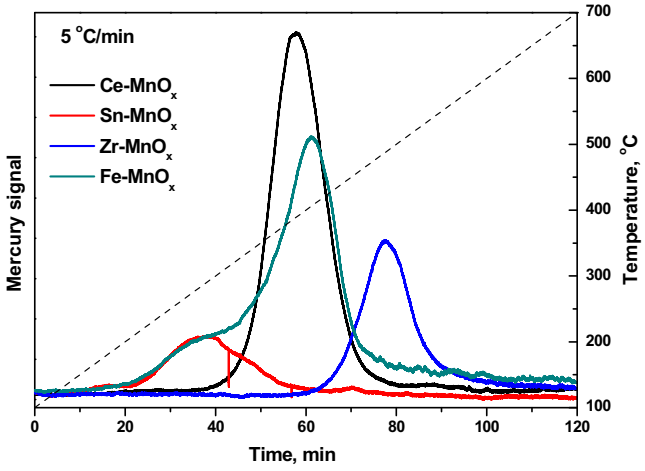

Fig. 5. Hg-TPD curves over Ce-MnO_x; Sn-MnO_x; Zr-MnO_x and Fe-MnO_x.

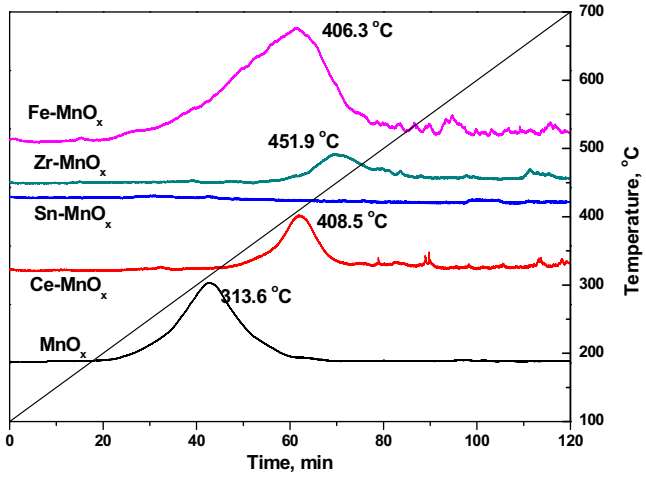

Fig. 6. Effect of SO_2 on Hg-TPD over various Mn-based materials.

The Hg-TPD spectra under the heating rates of 2 and 10 °C/min were presented in Figs. S2 and S3 . The mercury desorption temperature followed the order of Sn-MnO_x < Ce-MnO_x < Fe-MnO_x < Zr-MnO_x. It means that mercury binding intensity follows the same order. As presented in Table 1, the activation energy for desorption over these Mn-based binary oxides were calculated, they were 101.85, 46.32, 117.14, and 106.92 eV for Ce-MnO_x, Sn-MnO_x, Zr-MnO_x and Fe-MnO_x, respectively. Sn-MnO_x had the lowest energy due to its weak bond of mercury (Hg-O). While Zr-MnO_x had the highest energy indicated the strong bond of mercury (Hg≡O) on its surface. For Ce-MnO_x and Fe-MnO_x, the bond of mercry were similar to pure MnO_x. Mercury existed as of state of HgO over these two sorbents.

3.5. Effects of gas components on Hg-TPD spectra of Mn-based material

3.5.1. Effect of SO_2

SO_2 was the primary gas component in the coal-fired flue gas. It caused a reductive atmosphere which was not beneficial for Hg^0 removal. According to previous studies, Mn-based oxides can be easily poisoned by SO_2 [27–29]. Sulfate can generate on the surface of MnO_x which inhibited the active site for Hg^0 oxidation. The SO_2+Hg-TPD results are shown in Fig. 6. For MnO_x, the desorption peak centered at 313.6 °C. The desorption peak for Ce-MnO_x was at 408.5 °C. However, the area of desorption peak was smaller than

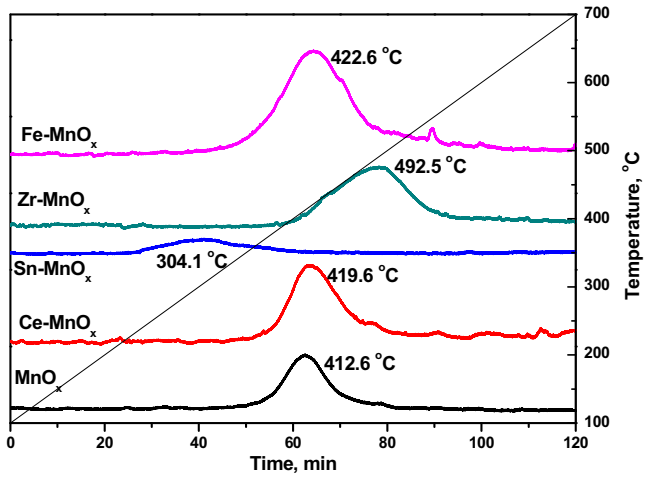

Fig. 7. Effect of NO on Hg-TPD over various Mn-based materials.

that of pure MnO_x. It could be speculated that SO_2 and HgO could reduce HgO to form Hg^0 in the simulated gas. $MnSO_4$ formed on the surface of Mn-based oxides. The equation was described as follows:

$$SO_2 + 1/2O_2 + HgO\text{-}Mn \rightarrow Hg^0 + MnSO_4 \quad (14)$$

Interesting, for Sn-MnO_x, the SO_2+Hg-TPD curve was nearly like a line. There was no peak on its curve. Sn-MnO_x was easily poisoned by SO_2 according to our previous work [20,21]. Additionally, the Hg-O presented a weak binding bond between mercury and oxygen. It can be easily re-reduced to Hg^0. For Zr-MnO_x, the desorption peak centered at 451.9 °C, part of oxidized mercury was reduced by SO_2, resulted in the smaller peak area. However, for Fe-MnO_x, it exhibited the resistance of SO_2 [21]. The peak area was larger than that of pure MnO_x, the existence of Fe protect Mn active sites from SO_2 poison. Moreover, the Fe-MnO_x and mercury had a strong bond (Hg≡O) with each other. Therefore, the weak bond of mercury can easily poisoned by SO_2, it was thought that the following reaction occurred between HgO and SO_3 [30]:

$$SO_2 + Hg\text{-}O \rightarrow Hg^0 + SO_3 \quad (15)$$

3.5.2. Effect of NO

The effect of NO on Hg-TPD was also investigated and the results are shown in Fig. 7. For pure MnO_x, a peak was centered at 412.6 °C, which was a little higher than that of under O_2. The MnO_x can adsorb NO to form NO_2 species which were beneficial for Hg^0 oxidation [18]. Ce-MnO_x had a similar peak compare to MnO_x and it was centered at 419.6 °C. For Sn-MnO_x, a small peak centered at 304.1 °C and there were no other peaks on its Hg-TPD curve. The results further indicated that mercury combined with the surface oxygen on Sn-MnO_x's surface. However, the peak area was smaller than that of MnO_x. The existence of NO could have a competitive adsorption effect. For Zr-MnO_x and Fe-MnO_x, the peaks were centered at 492.5 and 422.6 °C, respectively. Moreover, the peak area was not influenced when 500 ppm NO existed.

4. Conclusions

In this study, the desorption character of Mn-based oxide was investigated for a better understanding the binding state of mercury. The Hg-TPD results indicated that MnO_x had a better Hg^0 removal performance than AC due to the chemical-adsorption. After different elements modification, the Hg^0 removal performances were enhanced. However, mercury existed different binding state over these Mn-based oxides. Mercury existed as HgO on Mn-based oxides. But the binding strength was different. There is a weak bond (Hg-O) over Sn-MnO_x and a strong bond (Hg≡O) between mercury and Zr-MnO_x. The mercury on the surface of Ce-MnO_x and Fe-MnO_x was similar to that of pure MnO_x. SO_2 was not favorable for Hg^0 removal due to its poison effect on Mn active sites. NO was beneficial for Hg^0 removal because the surface oxygen can combine with NO to form nitrate which was useful for mercury sorption. According to the binding state of these Mn-based sorbents, it is significant to design novel materials for Hg^0 sorbents.

Acknowledgements

This study was supported by the Major State Basic Research Development Program of China (973 Program, No. 2013CB430005), and the National Natural Science Foundation of China (Nos. 51478261 and 51478261). Thanks for Shanghai Tongji Gao Tingyao Environmental Science and Technology Development Foundation. The work was also supported by China's Post-doctoral Science Fundation (No. 2015M581626).

Appendix A. Supplementary data

Supplementary data associated with this article can be found, in the online version, at http://dx.doi.org/10.1016/j.jhazmat.2016.09.030.

References

[1] S.M. Ullrich, T.W. Tanton, S.A. Abdrashitova, Mercury in the aquatic environment: a review of factors affecting methylation, Crit. Rev. Environ. Sci. Technol. 31 (2001) 241–293.
[2] E.G. Pacyna, J.M. Pacyna, F. Steenhuisen, S. Wilson, Global anthropogenic mercury emission inventory for 2000, Atmos. Environ. 40 (2006) 4048–4063.
[3] W.H. Schroeder, J. Munthe, Atmospheric mercury—an overview, Atmos. Environ. 32 (1998) 809–822.
[4] S. Wang, L. Zhang, G. Li, Y. Wu, J. Hao, N. Pirrone, F. Sprovieri, M. Ancora, Mercury emission and speciation of coal-fired power plants in China, Atmos. Chem. Phys. 10 (2010) 1183–1192.
[5] J.H. Pavlish, E.A. Sondreal, M.D. Mann, E.S. Olson, K.C. Galbreath, D.L. Laudal, S.A. Benson, Status review of mercury control options for coal-fired power plants, Fuel Process. Technol. 82 (2003) 89–165.
[6] H. Yang, Z. Xu, M. Fan, A.E. Bland, R.R. Judkins, Adsorbents for capturing mercury in coal-fired boiler flue gas, J. Hazard. Mater. 146 (2007) 1–11.
[7] M. Díaz-Somoano, S. Unterberger, K.R. Hein, Mercury emission control in coal-fired plants: the role of wet scrubbers, Fuel Process. Technol. 88 (2007) 259–263.
[8] A.A. Presto, E.J. Granite, Survey of catalysts for oxidation of mercury in flue gas, Environ. Sci. Technol. 40 (2006) 5601–5609.
[9] H. Zeng, F. Jin, J. Guo, Removal of elemental mercury from coal combustion flue gas by chloride-impregnated activated carbon, Fuel 83 (2004) 143–146.
[10] S.J. Lee, Y.-C. Seo, J. Jurng, T.G. Lee, Removal of gas-phase elemental mercury by iodine-and chlorine-impregnated activated carbons, Atmos. Environ. 38 (2004) 4887–4893.
[11] J. Liu, M.A. Cheney, F. Wu, M. Li, Effects of chemical functional groups on elemental mercury adsorption on carbonaceous surfaces, J. Hazard. Mater. 186 (2011) 108–113.
[12] C. Hu, J. Zhou, S. He, Z. Luo, K. Cen, Effect of chemical activation of an activated carbon using zinc chloride on elemental mercury adsorption, Fuel Process. Technol. 90 (2009) 812–817.
[13] E. Sasmaz, A. Kirchofer, A.D. Jew, A. Saha, D. Abram, T.F. Jaramillo, J. Wilcox, Mercury chemistry on brominated activated carbon, Fuel 99 (2012) 188–196.
[14] S.B. Ghorishi, R.M. Keeney, S.D. Serre, B.K. Gullett, W.S. Jozewicz, Development of a Cl-impregnated activated carbon for entrained-flow capture of elemental mercury, Environ. Sci. Technol. 36 (2002) 4454–4459.
[15] Y. Gao, Z. Zhang, J. Wu, L. Duan, A. Umar, L. Sun, Z. Guo, Q. Wang, A critical review on the heterogeneous catalytic oxidation of elemental mercury in flue gases, Environ. Sci. Technol. 47 (2013) 10813–10823.
[16] H. Xu, Z. Qu, S. Zhao, J. Mei, F. Quan, N. Yan, Different crystal-forms of one-dimensional MnO 2 nanomaterials for the catalytic oxidation and adsorption of elemental mercury, J. Hazard. Mater. 299 (2015) 86–93.
[17] G. Wang, H. Xu, L. Lu, H. Zhao, One-step synthesis of mesoporous MnO 2/carbon sphere composites for asymmetric electrochemical capacitors, J. Mater. Chem. A 3 (2015) 1127–1132.
[18] H. Xu, Z. Qu, C. Zong, F. Quan, J. Mei, N. Yan, Catalytic oxidation and adsorption of Hg 0 over low-temperature NH 3-SCR LaMnO 3 perovskite oxide from flue gas, Appl. Catal. B: Environ. 186 (2016) 30–40.
[19] C. He, B. Shen, J. Chen, J. Cai, Adsorption and oxidation of elemental mercury over Ce-MnO x/Ti-PILCs, Environ. Sci. Technol. 48 (2014) 7891–7898.

[20] J. Xie, H. Xu, Z. Qu, W. Huang, W. Chen, Y. Ma, S. Zhao, P. Liu, N. Yan, Sn–Mn binary metal oxides as non-carbon sorbent for mercury removal in a wide-temperature window, J. Colloid Interface Sci. 428 (2014) 121–127.
[21] H. Xu, J. Xie, Y. Ma, Z. Qu, S. Zhao, W. Chen, W. Huang, N. Yan, The cooperation of Fe Sn in a MnOx complex sorbent used for capturing elemental mercury, Fuel 140 (2015) 803–809.
[22] J. Xie, Z. Qu, N. Yan, S. Yang, W. Chen, L. Hu, W. Huang, P. Liu, Novel regenerable sorbent based on Zr–Mn binary metal oxides for flue gas mercury retention and recovery, J. Hazard. Mater. 261 (2013) 206–213.
[23] S.-j. Wu, R. Katayama, M. Azhar Uddin, E. Sasaoka, Z.-m. Xie, Study on reactivity of HgO over activated carbon with HCl and SO2 in the presence of moisture by temperature-programmed decomposition desorption mass spectrometry, Energy Fuels 29 (2015) 6598–6604.
[24] M.A. Lopez-Anton, R. Perry, P. Abad-Valle, M. Díaz-Somoano, M.R. Martínez-Tarazona, M.M. Maroto-Valer, Speciation of mercury in fly ashes by temperature programmed decomposition, Fuel Process. Technol. 92 (2011) 707–711.
[25] M. Ozaki, M.A. Uddin, E. Sasaoka, S. Wu, Temperature programmed decomposition desorption of the mercury species over spent iron-based sorbents for mercury removal from coal derived fuel gas, Fuel 87 (2008) 3610–3615.
[26] Z. Tan, L. Sun, J. Xiang, H. Zeng, Z. Liu, S. Hu, J. Qiu, Gas-phase elemental mercury removal by novel carbon-based sorbents, Carbon 50 (2012) 362–371.
[27] L. Ji, P.M. Sreekanth, P.G. Smirniotis, S.W. Thiel, N.G. Pinto, Manganese oxide/titania materials for removal of NO x and elemental mercury from flue gas, Energy Fuels 22 (2008) 2299–2306.
[28] J. Li, N. Yan, Z. Qu, S. Qiao, S. Yang, Y. Guo, P. Liu, J. Jia, Catalytic oxidation of elemental mercury over the modified catalyst Mn/α-Al2O3 at lower temperatures, Environ. Sci. Technol. 44 (2009) 426–431.
[29] N. Yan, W. Chen, J. Chen, Z. Qu, Y. Guo, S. Yang, J. Jia, Significance of RuO2 modified SCR catalyst for elemental mercury oxidation in coal-fired flue gas, Environ. Sci. Technol. 45 (2011) 5725–5730.
[30] M.A. Uddin, T. Yamada, R. Ochiai, E. Sasaoka, S. Wu, Role of SO 2 for elemental mercury removal from coal combustion flue gas by activated carbon, Energy Fuels 22 (2008) 2284–2289.